Outdoor MIMO Performance Evaluation for 28 and 73 GHz Ultra High Frequency Bands

Alauddin Al-Omary

University of Bahrain

aalomary@uob.edu.bh

Abstract

In this paper, the outdoor performance of Multiple Input Multiple Output (MIMO) systems for two ultra-high frequencies is analyzed. A simulation with realistic scenarios is set up using the Statistical Spatial Channel Model (SSCM) over frequency selective Rayleigh fading channel. The channel behavior of MIMO for two Ultra high frequencies (28 and 73 GHz) using different number of transmitter and receiver antenna, different receiver distance and different propagation scenario is investigated. Many parameters are calculated and compared to investigate the MIMO performance for these frequencies such as path loss, received power, directional and omni-directional Power Delay Profile (PDP) with strongest power, Angle of departure (AoD) and Angle of Arrival (AoA) power spectrum. The results are analyzed and a conclusion was drawn about the main characteristics and the usability of these ultra-high frequencies. The investigated frequencies are candidate to become a key component for cellular 5G networks and thus it is vital to investigate them to assist engineers in designing their 5G network.

Keywords: mm-Wave ,28 GHz, 73 GHz, MIMO, Statistical Spatial Channel Model (SSCM), Close-in path loss model, Outdoor propagation.

1. Introduction

As the race toward 5G strengthens, many new technologies are being introduced and tested. 5G is a high-tech evolution that will link our physical, virtual and social worlds. It will integrate multiple networks services, such as multimedia, virtual reality (VR) / augmented reality (AR), Machine-to-Machine (M2M) / Internet of Things (IoT), automotive, Smart City etc. The key requirement for 5G is to increase the capacity 1000 to 10000-time. This can be done by increasing network density, spectrum efficiency, and spectrum extension. High network density can be achieved by using small cells. Spectrum efficiency can be increased using massive MIMO and spectrum extension can be achieved using mmWave (above 5GHz) spectrum [1], [2], [3], [4], [5]. As the demand for more bandwidth is increasing, the massive spectrum available between 6 and 300 GHz is attractive solution. Several mmWave bands are currently being considered for global 5G networks. The 28- and 73-GHz frequency bands are getting attention by researchers and industry. These frequencies are relevant for outdoor communications as the attenuation loss induced from atmospheric absorption is minor over a realistic mmWave cell radius of 200 m [1]. Moreover, the Federal Communications Commission issued new rulemakings to get these bands into service [2], [3]. Extensive studies are necessary to determine coverage distances, path loss, and system configurations for mmWave wireless communications networks that will operate on 28 and 73 GHz. In this paper, the performance of Multiple Input Multiple Output (MIMO) systems for 28 GHz and 73 Ghz frequency is investigated. Many parameters are calculated and compared to investigate the MIMO performance for these frequencies. The results are analyzed and a conclusion was drawn about the main characteristics and usability of these ultra-high frequencies. The rest of the paper is organized as follows. Section 2 presents the literature review. In section 3, the scope of the paper is illustrated. Section 4 describe the Statistical Spatial Channel Model (SSCM). Section 5 outlines the simulation scenario. In Section 6 we evaluate and discuss the results. Finally, we summarize our contributions and draw conclusions.

2. Literature review

Major changes in system and network design will occur in 5G due to evolving innovative technologies, capacity of new spectra such as millimeter-wave (mmWave) frequencies [3], and new architectural concepts [4], [6]. Consequently it is essential to investigate mmWave to help engineers in their 5G network design. Channel characterization at both mmWave and centimeter-wave (cmWave) bands has been conducted by many prior researchers. Samsung early recognize the feasibility of mmWave for access in cellular systems [5] proposed one of the first studies of using mmWave as a key component for cellular 5G networks. Researchers in [6] introduce scenarios for outdoor access based on propagation measurements at 28, 38, 60 and 73 GHz. In [7], researchers studied the effectiveness of beamforming and Multi User MIMO in mmWave bands for system rate improvements. Researchers at [8] proposed the concept of mmWave networks overlaying to convert small-cells to larger macro-cells. This concept is one of the model system architecture of current 5G standardizations. The authors in [9]–[11] studied and modeled the UMi and indoor channels at 28 GHz and 60 GHz. It is very likely that 28 GHz will be used for the first 5G deployments in the South Korea, US and Japan beside that 28GHz, 38Ghz, 60 GHz and 73 GHz are strong candidate bands for implementing 5G networks [1], [3]. The 28- and 73-GHz frequency bands for outdoor communications have advantages of less attenuation loss induced from atmospheric absorption when compared with other ultra-high bands (38 and 60). It was reported to have attenuation loss of less than 0.1 dB over a realistic mmWave cell radius of 200 m [12], [13] while it is significantly higher at 60 GHz (~4 dB/200 m).

3. Scope of the work

Our main contribution is the investigations of outdoor-to-outdoor MIMO channel performance estimation using the Close-In (CI) path loss model and frequency selective Rayleigh fading channel. We study the channel behavior for two Ultra high frequencies (28 and 73 GHz) using different number of transmitter and receiver antennas, different receiver distances and different propagation scenario. Many parameters are calculated and compared to investigate the MIMO performance for these frequencies such as path loss, received power, coverage distance, directional and omni-directional Power Delay Profile (PDP) with strongest power, Angle of departure (AoD) and Angle of Arrival (AoA) power spectrum. Calculating and analyzing these parameters are important and will help researchers and engineers in understanding the behavior of these new frequencies and help them in designing 5G networks.

4. Channel Model

Two kinds of channel models are widely used to evaluate the performances of the wireless communication systems. These are namely, correlation-based stochastic models (CBSMs) and geometry-based stochastic models (GBSMs) . Because of its low complexity, the CBSMs model is mainly used for analyzing the theoretical performance of MIMO systems. The accuracy of CBSMs is also limited for the realistic MIMO system and it is difficult to model wireless channels considering the non-stationary phenomenon and spherical wave effects. In contrast, the GBSMs model has higher computation complexity but it has more accuracy, can accurately reflect the realistic channel properties, and is more suitable for massive MIMO channel.

4.1 Statistical Spatial Channel Model

In this paper, a GBSMs-like model channel developed at New York university [14], [15], [16], [17] called the Statistical Spatial Channel Model (SSCM) is used to model the MIMO channel . SSCM is a multi-frequency 3-dimensional (3-D) measurement-based channel impulse response (CIR) model [14]. Like the 3GPP channel model SSCM supports arbitrary carrier frequency, RF bandwidth, and antenna beam width for both omnidirectional and arbitrary directional antennas. SSCM has been used successfully in modeling mmWave channels [18]. It make use of time clusters (TC) and spatial lobes (SL) to model the omnidirectional CIR and corresponding joint angle of departure (AOD)/angle of arrival (AOA) power spectra. Time clusters are composed of multipath components (MPCs) traveling closely in time. MPCs arrive from potentially different angular directions in a short excess delay time window. Spatial lobes represent main directions of arrival (or departure) where energy arrives over several hundreds of nanoseconds. Multiple paths within a TC can arrive at unique pointing angles [18] and can be detected due

to high gain directional antennas. As was reported in [18], the TCSL approach implements a physically-based clustering scheme. The time-partitioning methodology delineates the beginning and end times of each time cluster, using a 25ns minimum inter-cluster void interval. Sequentially arriving MPCs that occur within 25 ns of each other are assumed to belong to one TC.
To represent the radio propagation channel between a transmitter and receiver the double-directional omnidirectional CIR is commonly used. It can be expressed as in eq. (1) [17], [21]:

$$h_{omni}\,(t,\Theta,\phi) = \sum_{n=1}^{N}\sum_{m=1}^{Mn} a_{m,n}\;\; e^{j\varphi_{m,n}}\,.\,\delta\left(t-\tau_{m,n}\right).\,\delta\left(\Theta-\Theta_{m,n}\right).\,\delta\left(\phi-\;\phi_{m,n)}\right) \quad (1)$$

where t denotes absolute propagation time, $\boldsymbol{\Theta}=(\boldsymbol{\theta},\boldsymbol{\phi})_{\mathrm{TX}}$, and $\boldsymbol{\phi}=(\boldsymbol{\theta},\boldsymbol{\phi})_{\mathrm{RX}}$ are the vectors of azimuth/elevation AODs and AoAs, respectively. N and Mn denotes the number of time clusters (defined in [17]), and the number of cluster subpaths, respectively. $a_{m,n}$ is the amplitude of the mth subpath belonging to the n^{th} time cluster; $\boldsymbol{\varphi_{m,n}}$and $\boldsymbol{\tau_{m,n}}$ are the phases and propagation time delays, respectively; $\boldsymbol{\Theta_{m,n}}$ and $\boldsymbol{\phi_{m,n)}}$ are the azimuth/elevation AODs, and azimuth/elevation AOAs, respectively, of each multipath component.
The joint AOD-AOA power spectra $P(\boldsymbol{\Theta},\boldsymbol{\phi})$ in 3-D can be obtained by integrating the magnitude squared of (1) over the propagation time dimension,

$$P(\Theta,\phi) = \int_0^{\infty} |h(\,t,\Theta,\phi)|^{\,2}\,dt \quad (2)$$

$$P(\Theta,\phi) = \sum_{n=1}^{N}\sum_{m=1}^{Mn} |a_{m,n}\,|^{\,2}.\,\delta\left(\Theta-\Theta_{m,n}\right).\,\delta\left(\phi-\;\phi_{m,n)}\right) \quad (3)$$

The *directional* PDPs at a desired TX-RX unique antenna-pointing angle, and for arbitrary TX and RX antenna patterns can be obtained by partitioning the omnidirectional CIR to yield,

$$h_{dir}\,(t,\Theta_d,\phi_d) = \sum_{n=1}^{N}\sum_{m=1}^{Mn} a_{m,n}\;\; e^{j\varphi_{m,n}}\,.\,\delta\left(t-\tau_{m,n}\right).\;g_{TX}\left(\Theta_d-\Theta_{m,n}\right).\,g_{RX}\,(\phi_d-\;\phi_{m,n)} \quad (4)$$

where $(\,\Theta_d,\phi_d)$ are the desired TX-RX antenna pointing angles, $g_{TX}(\Theta)$ and $g_{RX}(\phi)$are the arbitrary 3-D (azimuth and elevation) TX and RX complex amplitude antenna patterns of multi-element antenna arrays, respectively. The directional PDP is obtained in eq. (4) by amplifying the power levels of all multipath components lying close to the desired pointing direction. The power levels of multipath components lying far away from the desired pointing direction is set to 0 [17].

4.2 Path Loss Model
In this paper, the close-in free space reference distance (CI) path loss model with a 1 m reference distance is used [22], [23], [26], [25]. The path loss is expressed as:

$$PL^{CL}\,(f,d)[dB] = FSPL\,(f,1m)[dB] + 10nlog_{10}\,(d) + AT[dB] + \;X_{\sigma}^{CL}\,, \quad (5)$$

$$\text{Where d} \;\geq\; 1\text{m}$$

where f denotes the carrier frequency in GHz, d is the 3D T-R separation distance, n represents the path loss exponent (PLE), AT is the attenuation term induced by the atmosphere, $X_{\sigma}^{CL}$is a zero-mean Gaussian random variable with a standard deviation σ in dB. FSPL(f, 1m) denotes the free space path loss in dB at a T-R separation distance of 1 m at the carrier frequency f:

$$FSPL(f, 1m)[dB] = 20\ log_{10}\left(\frac{4\pi f \times 10^9}{c}\right) \qquad (6)$$

$$= 32.4[db] + 20\ log_{10}(f)$$

where c is the speed of light in a vacuum, and f is in GHz.
The term AT is characterized by:

$$AT[dB] = \alpha\ [dB\ /m] \times d\ [m] \qquad (7)$$

where α is the attenuation factor in $dB\ /m$ for the frequency range of 1 GHz to 100 GHz, which includes the collective attenuation effects of dry air (including oxygen), water vapor, rain, and haze [23]. The parameter d is the 3D T-R separation distance in (1).

5. Simulation methods and Parameters

The channel behavior of the two Ultra high frequency bands (28GHz and 73 GHz) was studied using NYUSIM simulator [29]. NYUSIM is a MATLAB-based statistical simulator that can be used to generate realistic temporal and spatial channel responses to support realistic physical- and link-layer simulations and design for fifth-generation (5G) cellular communications. NYUSIM is built upon the statistical spatial channel model [17] for broadband millimeter-wave (mmWave) wireless communication systems developed by researchers at New York University (NYU).

5.1 Simulation Scenario

We investigate the outdoor MIMO performance for 28 GHz and 73 GHz frequency bands. Different realistic scenarios that cover many aspects of MIMO system using the proposed channel models are conducted. These include simulation using different numbers of transmitter and receiver antennas, different types of antennas, different separation distance between transmitters and receivers, and different transmission environments as shown below:

1- Transmitter antenna elements are set to (16, 32, 64) and receiver antenna elements are set to (1, 4, 8) respectively.
2- Two types of antennas are used, uniform linear array (ULA) and Uniform Rectangular Array (URA).
3- Separation distance between transmitter and receiver is set to (50, 100, 150, 200, 250, 300, 350, 400, 450,500 m)
4- Two types of Transmission environment are investigated (LoS and NLoS).

The following parameters are calculated and compared for each of the above-mentioned cases:

a. Path loss
b. Path loss exponent
c. Coverage distance
d. Directional Power delay profile (PDP) with strongest power,
e. Omni-directional PDP
f. Angle of departure (AoD) power spectrum
g. Angle of Arrival (AoA) power spectrum

5.2 Simulation parameters

The following input parameters settings were used to run a simulation:

5-2-1 Fixed parameters

- Base station antenna height: 35 m
- RF bandwidth: 800 MHz
- Scenario: UMi
- TX Power: 30 dBm

- Barometric Pressure: 1013.25 mbar
- Humidity: 50%
- Temperature: 20 ° C
- Rain Rate: 0 mm/hr
- Polarization: Co-Pol
- Foliage Loss: No
- TX Antenna Spacing: 0.5 wavelength
- RX Antenna Spacing: 0.5 wavelength
- Number of TX Antenna Elements Per Row Wt: 2
- Number of RX Antenna Elements Per Row Wr: 2
- TX Antenna Azimuth HPBW: 10.9° for ULA and 7° for URA
- TX Antenna Elevation HPBW: 8.6 ° for ULA and 7° for URA
- RX Antenna Azimuth HPBW: 10.9° for ULA and 7° for URA
- RX Antenna Elevation HPBW: 8.6 ° for ULA and 7° for URA

5-2-2 Variable parameters
The variable simulation parameters are shown in table (1)

Table (1) The variable simulation parameters

Frequency	28Ghz						73GHz					
No of Tx Antenna	16		32		64		16		32		64	
No of Rx Antenna	1		4		8		1		4		8	
Distance between Tx and RX	50-500m		50-500m		50-500m		50-500m		50-500m		50-500m	
Environment	LoS	NLoS	LoS	NLoS	LoS	NLoS	LoS	NLoS	LoS	NLoS	LoS	NLoS
Antenna Type	ULA	URA	ULA	URA	ULA	URA	ULA	URA	ULA	URA	ULA	URA
No of locations for receivers	10 locations											
No of rounds	10 rounds for each location											

6. Simulation Results and discussion

The parameters mentioned in section 4.1 were calculated. These parameters are analyzed to draw conclusion about the performance of MIMO system with different antenna configuration using 28GHz and 73 GHz.

6.1 Directional PDP, Omni-directional PDP and corresponding DOA and AOA
Ten rounds of simulation were conducted to calculate the Power delay profiles (PDP). In each round, the PDP for 10 transmitter-receiver locations, were calculated. This cover distances ranging from 50m to 500m and using different antenna configuration (16X1, 32X4, 64X8). Key parameters for each of the directional PDPs are calculated. This includes time delay, received power, phase, azimuth and elevation AODs and AOAs of each resolvable MPC (i.e., antenna pointing angle), along with directional path loss and directional RMS delay spread. Figure (1) shows sample of directional PDP with strongest power for 32X4 (32 Tx antenna and 4 Rx antenna) with 300 m distance separation between Tx and RX using 28GHz frequency band. Figure (2) shows sample of directional PDP for the same antenna configuration using 73 GHz frequency band. In figure (1) and (2), the transmitted signals from 32 antenna were grouped in 4 clusters separated in time and the strongest received power in case of 28GHz frequency was -33.6 dBm

with path loss of 111.3 dB. For 73 GHz, the strongest received power was -40.9 dBm with path loss of 120.7 dB. As was shown from these figures, increasing the frequency cause increase in path loss and the received power is decreased accordingly. This go well in accordance to equation (5) and (6) in section (4.1) and means that using the 73GHz frequency band needs more transmitting power than the 28GHz band.

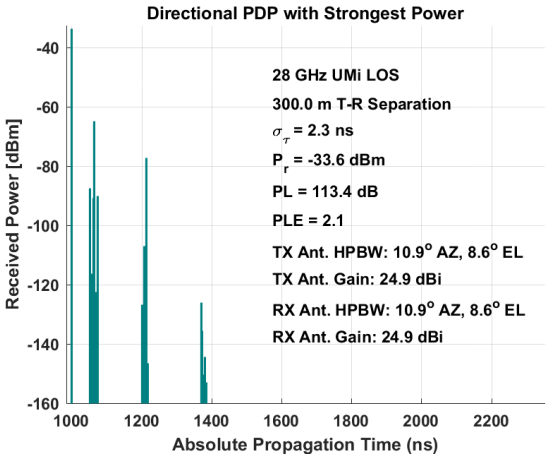

Fig. (1) Directional PDP for 32X4 LOS 28GHz

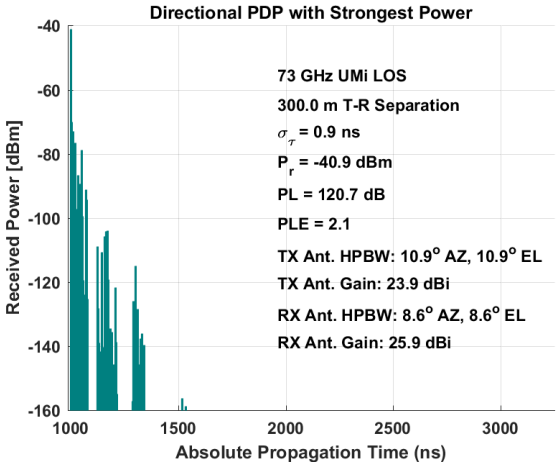

Fig. (2) Directional PDP for 32X4 LOS 73GHz

Figure (3) illustrates an omnidirectional PDP, where there are 32 multipath taps which are grouped into exponentially decaying four time clusters. The four multipath taps are grouped into four spatial lobes in AOD and AOA spectrum, as shown in Fig. (4) and fig. (5). These figures show the departed and received signal components and the highest power lobe. The information extracted from AOD and AOA calculation help cellular designers in building antenna arrays and beam steering algorithms that can maximize signal strength, thus improving signal quality and system capacity.

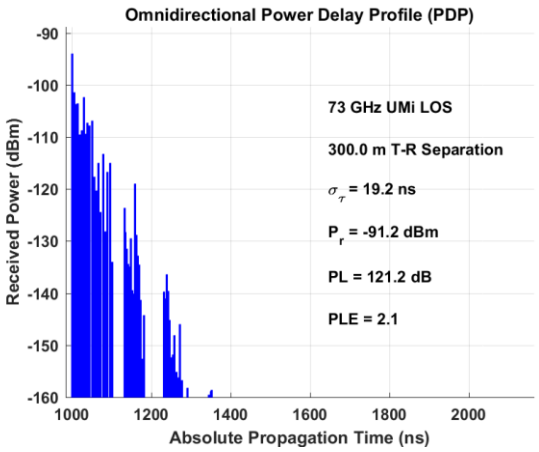

Figure (3) Omni-directional PDP

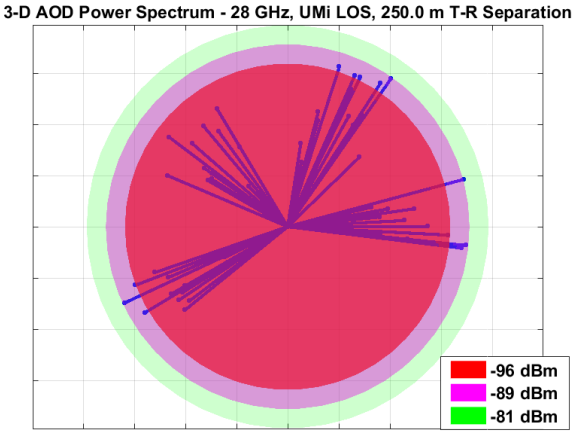

Figure (4) Sample of AOD Power Spectrum

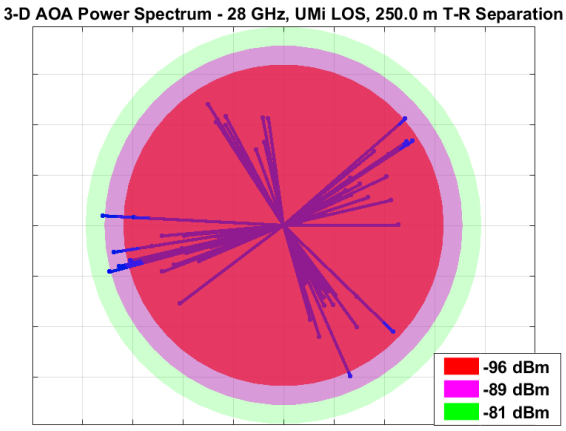

Figure (5) Sample of AOA power Spectrum

6.2 Path Loss

Path loss and path loss exponent (PLE) are important parameters that influence the quality of the link. These parameters if accurately calculated lead to efficient design and operation of wireless networks. They are also significant in considering other issues in communications such as localization, energy-efficient routing, and channel access. Figures (6) and (7) show the calculated path loss for 28GHz and 73GHz frequency bands. In generating these figures, the Tx and Rx antennas azimuth and elevation HPBWs are set to 10.9º and 8.6º, respectively for LOS antenna and for NLOS antenna azimuth and elevation HPBWs are set to 7 º as was used in [13], [14]. The values in these figures are generated from 100 continuous simulation runs over a distance range of 50m to 500m. In addition to path loss, the fitted Path Loss Exponent (PLE) and shadow fading standard deviation are calculated using the minimum-mean-square-error (MMSE) method [13], [14]. In Figures (6), (7), n denotes the PLE, σ_{omni} , σ_{dir} , $\sigma_{dir\text{-}best}$ is the shadow fading standard deviation," omni" denotes omnidirectional, "dir." represents directional, and "dir-best" means the direction with the strongest received power. When comparing figure (6) and figure (7), it is shown that the path loss for 73 GHz frequency band is more than that of 28 GHz with a magnitude of about 10dB. This is clear as path loss is proportional to frequency as stated by equation (5) and (6) in section 4.1. In figure (6), the omnidirectional PLE (n_{omni}) is 1.9 and the directional PLE (n_{dir}) is 2.9 and direction best PLE ($n_{dir\text{-}best}$) is 2.1 with respect to a 1 m close-in free space reference distance. The directional path loss and directional PLE are more lossy than the omnidirectional case. This is because the directional antenna will spatially filter out many MPCs due to its directional pattern, such that the Rx receives fewer MPCs hence less energy, thereby the directional path loss is higher after removing the antenna gain effect from the received power [12], [17]. However, in figure (6), the calculated directional path loss exponents is calculated considering arbitrary unique pointing angles, but when searching for the strongest Tx-Rx angle pointing link at each Rx location it was decreased from 2.9 to 2.1 ($\sigma_{dir\text{-}best}$ in figure 6). This shows great significance of beamforming at the base station and mobile handset for SNR enhancement and increasing the coverage distance.

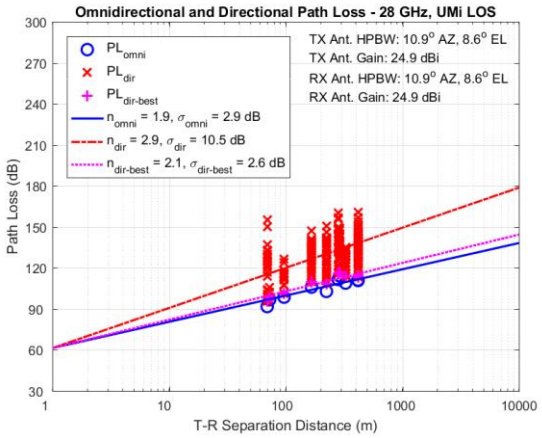

Figure (6) Path loss for 28GHz band (LOS)

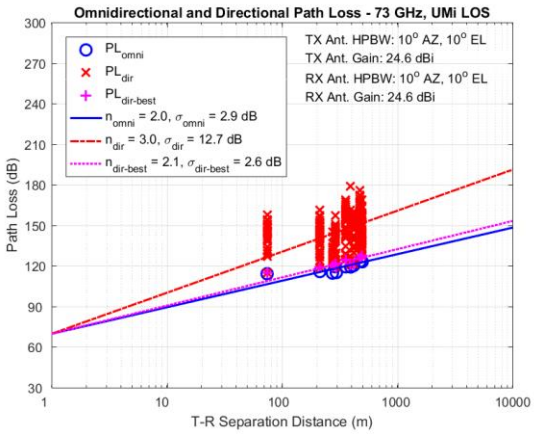

Figure (7) Path loss for 73GHz (LOS)

6.3 Coverage distance

In order to investigate the allowable coverage distance for 28 GHz and 73 GHz frequency bands, many simulation rounds are conducted using different separation distances between Transmitter and receiver (50-1000m). Besides that, the simulation round are done using different scenario (LOS , NLOS) and different antenna (ULA and URA). Table (2) shows the different dBm signal strength and their signal status [17]. It is obvious from the table that -60 dBm is good reliable signal and -67 dBm is the minimum for voice and non-HD video signal[1].

Table (2)

Received Signal power strength	Signal status
-30 dBm	Perfect signal
-50 dBm	Excellent signal
-60 dBm	Good reliable signal
-67 dBm	Minimum for Voice and non-HD signal
-70 dBm	Light browsing and email
-80 dBm	Unstable signal
-90 dBm	Unlikely connection

Table (3) shows the summary results of received power (Pr) in dBm for a distance of 500m. The 500 m distance is critical because beyond this value the received power in some cases will be dropped below – 60 dB, which is considered as, nearly perfect value of received power. From table (3) we can notice the following cases:

[1]https://www.cisco.com/c/en/us/td/docs/solutions/Enterprise/Borderless_Networks/Unified_Access/CMX/CMX_RFFund.pdf

Case 1: Using LOS the 500-coverage distance for both 28 GHz and 73 GHz is guaranteed and even can be increased little more beyond 500m. This is true for both ULA and URA antenna.

Case 2: Using NLOS the received power for 28GHz frequency is still good for URA antenna but for ULA antenna all the received power are slightly less than -60dBm but it is still within the acceptable range and can be detected so the 500-coverage area may be ok for 28GHz.

Case 3: Using NLOS, for 73 GHz all the received power will be less than -60 dB by different margin using ULA or URA antenna and 500m-coverage may be risky.

Table (3) Received power for different frequencies and MIMO scenario

Frequency	MIMO Antenna Tx X Rx	Pr in dBm (LOS)/ ULA	Pr in dBm (LOS) / URA	Pr in dBm (NLOS)/ ULA	Pr in dBm (NLOS) / URA
28 GHz	16X1	-43.1	-38.5	-70.2	-63.2
	32X4	-37.2	-33.3	-68.1	-57.3
	64X8	-34	-31.2	-66.3	-53.1
73GHz	16X1	-53.3	-48.5	-75.1	-70.3
	32X4	-48.7	-45.1	-72.2	-68.2
	64X8	-42.3	-40.6	-71.4	-65.4

6.4 The effect of massive antenna

Figure (8) shows the received power for different antenna configuration (16X1, 32X4 and 64X8) using 28 GHz LOS scenario. It is shown form the figure that as the number of antenna increases, the received power (in dBm) becomes better. Using many antennas separated at certain distance from each other make each antenna receives a slightly different version of the signal sent by the transmitter. The receiver combines them to form a better estimate of the transmitted signal as compared with the case of one receiving antenna. Moreover, with the increase in the number of BS antennas, the random channel vectors between the users and the base station become pair wisely orthogonal. Uncorrelated noise and intracell interference can be removed completely with simple matched filtering techniques. As it was shown in figure (8) an average increase in performance of about 5dBm has been achieved when increasing the number of antenna from 16X1 to 64X8.

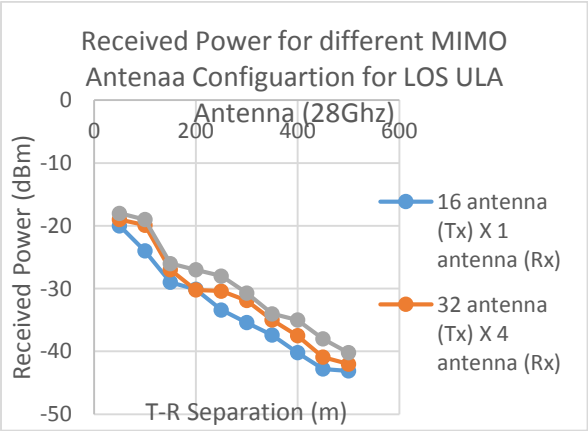

Figure (8) Effect of increasing number of antenna at Tx and Rx

6.5 ULA Vs. URA antenna Performance

Figure (9) shows the received power using two types of antenna (ULA and URL). It is shown from the figure that the URA antenna gives better performance than ULA antenna of about 4 dBm on average. The URA antenna consists of identical antenna elements which are arranged in an equally spaced rectangular grid. Therefore, a URA is capable of resolving the angles of incoming wave fronts in azimuth and elevation. This feature make the URA more effective than ULA antenna.

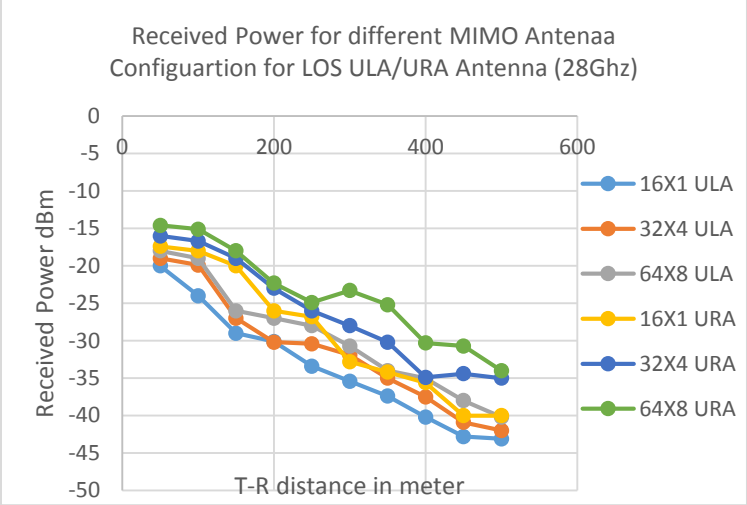

Figure (9) The received power using two types of antenna (ULA and URL)

6.6 LOS Vs NLOS Transmission

Figure (10) shows the received power using LOS ULA/URA antenna and figure (11) shows the received power using NLOS ULA /URA antenna. It is shown from these figures that LOS gives better received power, as the power is concentrated in one direction rather than distributing the same power in many directions. However, in LOS antenna the transmitted power need to be directed to the receiver using beamforming techniques to steer the beam to the dominant path at the transmit and receive ends by searching for the strongest TX-RX angle pointing link at each RX location. Thus, LOS antenna are more complex than NLOS antenna but is more effective in achieving more data rate transmission.

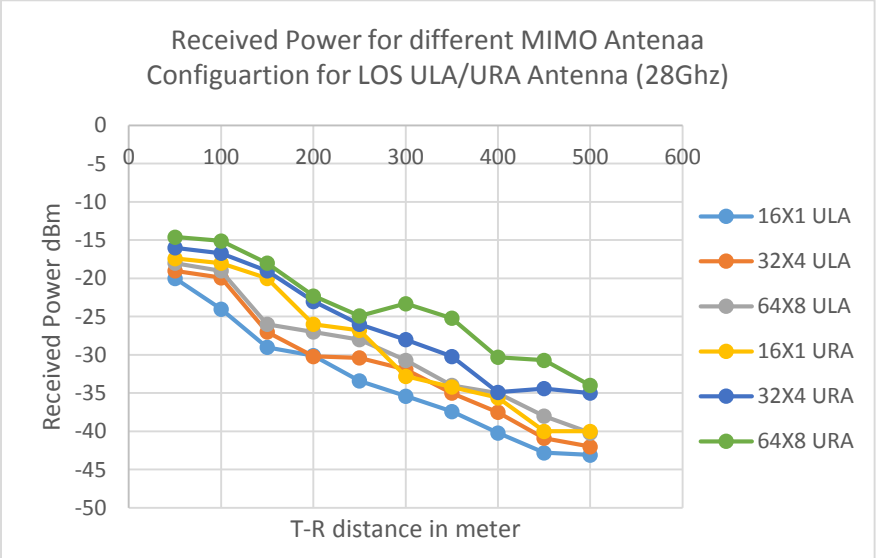

Figure (10) The received power using LOS ULA/URA antenna

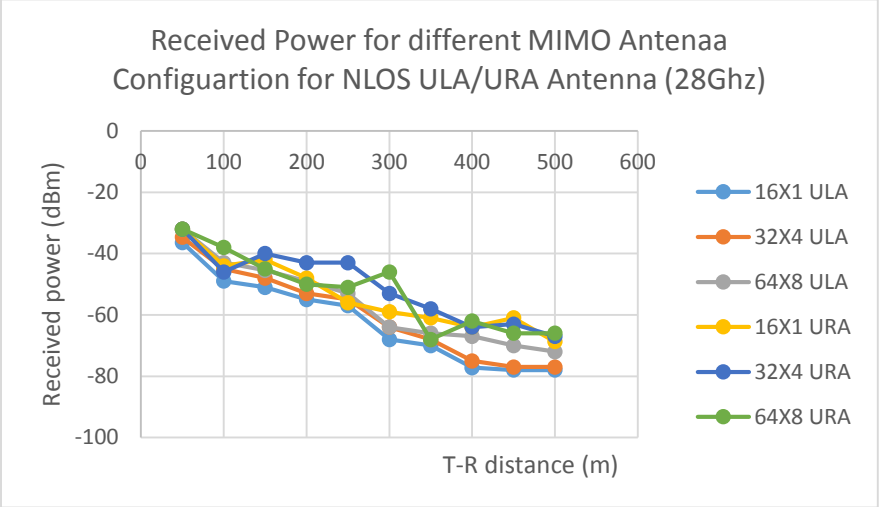

Figure (11) The received power using NLOS ULA /URA antenna

Conclusion

As the race toward 5G networks intensify, the wireless spectrum below 6 GHz will not be enough to meet future 5G network needs. Several mmWave bands are currently being considered for global 5G networks. In this paper, the performance of Multiple Input Multiple Output (MIMO) systems for 28 GHz and 73 GHz frequency bands for outdoor communications are investigated to check their relevance for 5G. Different realistic scenarios that cover many aspects of MIMO system using the Statistical Spatial Channel Model are conducted. Many important parameters are calculated and compared such as path loss, coverage distance, directional and omnidirectional PDP, AOD and AOA to investigate the MIMO performance at these frequencies. Investigation has shown that the coverage distances of the new frequencies for most of the cases can be good within a distance of 500m if a suitable transmitting power (about 30dBm) is used at the transmitter site. Path loss increases for these new bands and more dense cells are suitable to compensate for this extra path loss. The path loss for 73GHz is reported to be more than 28 GHz by amount of 10 dB on average. Directional and omni-directional Power Delay Profile are calculated with key parameters for each PDPs, along with directional path loss and directional RMS delay spread. These parameters are necessary for understanding inter-symbol interference (ISI) effects of the channel that could cause heavy data loss in the communication especially in faded channels. It was shown that the directional path loss and directional PLE are more lossy than the omnidirectional case. This is because the directional antenna will spatially filter out many MPCs due to its directional pattern, such that the Rx receives fewer MPCs hence less energy, thereby the directional path loss is higher after removing the antenna gain effect from the received power. The directional path loss exponents were calculated to be 2.9 and 3 at 28 GHz and 73 GHz, respectively, when considering arbitrary unique pointing angles, but were decreased to 2.1 when searching for the strongest Tx-Rx angle pointing link at each Rx location. This shows the significance of beamforming at the base station and mobile handset for SNR enhancement and increasing the coverage distance. In investigating the LOS and NLOS case, it was shown that LOS gives better received power, as the power is concentrated in one direction rather than distributing the same power in many directions. The comparison between ULA and URA antenna shows the URA antenna gives better performance than ULA antenna of about 4 dbm on average. The URA antenna consists of identical antenna elements, which are arranged, in an equally spaced rectangular grid. Therefore, a URA is capable of resolving the angles of incoming wave fronts in azimuth and elevation. This feature makes the URA more effective than ULA antenna. The investigation of 28GHz and 73 Ghz frequencies presented in this paper will be helpful in

understanding the mmWave system-wide behavior and radio-system design in outdoor environments for next generation 5G communication systems.

References

[1] Anass Benjebbour, "5G access technology", NTT DOCOMO Technical Journal, Vol 17, No. 4, pp 16-28, 2016.

[2] Federal Communications Commission, "Report and Order and Further Notice of Proposed Rulemaking," FCC 16-89, July 2016.

[3] FCC News, "FCC takes steps to facilitate mobile broadband and next generation wireless technologies in spectrum above 24 GHz," July 2016. Available online: http://transition.fcc.gov/Daily_Releases/Daily_Business/2016/db0 714/DOC 340301A1.pdf

[4] ITU-R, "IMT Vision – Framework and overall objectives of the future development of IMT for 2020 and beyond," Recommendation M. 2083-0, Sep. 2015.

[5] 3GPP TR22.891, "Study on New Services and Markets Technology Enablesr," V14.2.0, Sep. 2016.

[6] Z. Pi and F. Khan, "An introduction to millimeter-wave mobile broadband systems," IEEE Communications Magazine, vol. 49, no. 6, pp. 101-107, June 2011.

[7] S. Rangan, T.S. Rappaport, E. Erkip, "Millimeter-wave Cellular Wireless Networks: Potentials and Challenges." Proc. IEEE, vol. 102, no. 3, pp. 366-385, Mar. 2014.

[8] T. Bai, A. Alkhateeb, R.W. Heath, "Coverage and capacity of millimeter-wave cellular networks," IEEE Commun. Mag., vol. 52, no. 9, pp. 70-77, Sep. 2014.

[9] K. Sakaguchi, G.K. Tran, H. Shimodaira, S. Nanba, T. Sakurai, K. Takinami, I. Siaud, E.C. Strinati, A. Capone, I. Karls, R. Arefi, and T. Haustein, "Millimeter-wave Evolution for 5G Cellular Networks," IEICE Trans. Commun, vol. E98-B, no. 3, pp. 338- 402, Mar. 2015.

[10] P. Soma, Y. Chia, and L. Ong, "Modeling and analysis of time varying radio propagation channel for lmds," in 2000 IEEE Radio and Wireless Conference (RAWCON 2000), 2000, pp. 115–118.

[11] S. Geng, J. Kivinen, X. Zhao, and P. Vainikainen, "Millimeter-wave propagation channel characterization for short-range wireless communications," IEEE Transactions on Vehicular Technology, vol. 58, no. 1, pp. 3–13, Jan 2009.

[12] T. S. Rappaport et al., "Millimeter wave mobile communications for 5G cellular: It will work!" IEEE Access, vol. 1, pp. 335–349, May 2013.

[13] 5G Channel Model for bands up to 100 GHz, Annex A: Summary of channel sounding, simulations and measurement data, March 2016. Available online: http://www.5gworkshops.com/Annex%20for%205G%20channel%20model%20for%20bands%20up%20to%20100%20GHz%20-%20Second%20revision.pdf

[14] M. K. Samimi and T. S. Rappaport, "3-D millimeter-wave statistical channel model for 5G wireless system design," IEEE Transactions on Microwave Theory and Techniques, vol. 64, no. 7, pp. 2207–2225, July, 2016.

[15] M. K. Samimi, T. S. Rappaport, and G. R. MacCartney, Jr., "Probabilistic omnidirectional path loss models for millimeter-wave outdoor communications," in IEEE Wireless Communications Letters, vol. 4, no. 4, Aug. 2015, pp. 357–360.

[16] M. K. Samimi and T. S. Rappaport, "Ultra-wideband statistical channel model for non line of sight millimeter-wave urban channels," in 2014 IEEE Global Communications Conference (GLOBECOM), Dec. 2014, pp. 3483–3489.

[17] M. K. Samimi and T. S. Rappaport, "Statistical Channel Model with Multi-Frequency and Arbitrary Antenna Beamwidth for Millimeter-Wave Outdoor Communications,," in 2015 IEEE Global Communications Conference (GLOBECOM) Workshop, Dec. 2015.

[18] T. S. Rappaport et al., "Millimeter wave mobile communications for 5G cellular: It will work!" IEEE Access, vol. 1, pp. 335–349, 2013.

[19] T. S. Rappaport et al., "Broadband millimeter-wave propagation measurements and models using adaptive-beam antennas for outdoor urban cellular communications," IEEE Transactions on Antennas and Propagation, vol. 61, no. 4, pp. 1850–1859, April 2013.

[20] K. L. Blackard, M. J. Feuerstein, T. S. Rappaport, S. Seidel, and H. Xia, "Path loss and delay spread models as functions of antenna height for microcellular system design," in 1992 IEEE 42nd Vehicular Technology Conference, May 1992, pp. 333–337 vol.1.
[21] M. Steinbauer, A. F. Molisch, and E. Bonek, "The double-directional radio channel," IEEE Antennas Propag. Mag., vol. 43, no. 4, pp. 51–63, Aug. 2001.
[22] T. S. Rappaport et al., "Wideband millimeter-wave propagation measurements and channel models for future wireless communication system design (Invited Paper)," IEEE Transactions on Communications, vol. 63, no. 9, pp. 3029–3056, Sep. 2015.
[23] S. Sun et al., "Investigation of prediction accuracy, sensitivity, and parameter stability of large-scale propagation path loss models for 5G wireless communications," IEEE Transactions on Vehicular Technology, vol. 65, no. 5, pp. 2843–2860, May 2016.
[24] H. J. Liebe et al., "Propagation modeling of moist air and suspended water/ice particles at frequencies below 1000 GHz," AGARD Conference Proceedings 542, May 1993.
[25] T. S. Rappaport, R. W. Heath, Jr., R. C. Daniels, and J. N. Murdock, Millimeter Wave Wireless Communications. Pearson/Prentice Hall 2015.
[26] G. R. MacCartney, Jr. et al., "Indoor office wideband millimeter-wave propagation measurements and channel models at 28 and 73 GHz for ultra-dense 5G wireless networks," IEEE Access, vol. 3, pp. 2388–2424, Oct. 2015.
[27] G. R. MacCartney, Jr. and T. S. Rappaport, "Study on 3GPP rural macrocell path loss models for millimeter wave wireless communications, in 2017 IEEE International Conference on Communications (ICC), May 2017, pp. 1–7.
[28] H. J. Liebe et al., "Propagation modeling of moist air and suspended water/ice particles at frequencies below 1000 GHz," AGARD Conference Proceedings 542, May 1993.
[29] S. Sun, G. R. MacCartney Jr., and T. S. Rappaport, "A novel millimeter-wave channel simulator and applications for 5G wireless communications," 2017 IEEE International Conference on Communications (ICC), Paris, May 2017.